Human Molecular Genetics, 2016, Vol. 25, No. 17 3741–3753

doi: 10.1093/hmg/ddw220
Advance Access Publication Date: 8 July 2016
Original Article

ORIGINAL ARTICLE

Loss-of-function mutations in the *SIGMAR1* gene cause distal hereditary motor neuropathy by impairing ER-mitochondria tethering and Ca^{2+} signalling

Elisa Gregianin[1,†], Giorgia Pallafacchina[2,†], Sofia Zanin[2], Valeria Crippa[3], Paola Rusmini[4], Angelo Poletti[4], Mingyan Fang[5], Zhouxuan Li[5], Laura Diano[6], Antonio Petrucci[7], Ludovico Lispi[7], Tiziana Cavallaro[8], Gian M. Fabrizi[8], Maria Muglia[9], Francesca Boaretto[1], Andrea Vettori[1], Rosario Rizzuto[2], Maria L. Mostacciuolo[1] and Giovanni Vazza[1,*]

[1]Department of Biology, University of Padova, [2]Department of Biomedical Sciences, University of Padova and CNR Neuroscience Institute, Padova, Italy, [3]Experimental Neurobiology Lab, IRCCS "C. Mondino" National Neurological Institute, Pavia, Italy, [4]Department of Pharmacological and Biomolecular Sciences, Università degli Studi di Milano, Milan, Italy, [5]Department of Science & Technology, BGI-Shenzhen, Shenzhen, China, [6]Medical Genetics, University Hospital "Tor Vergata", Roma, Italy, [7]Neuromuscular and Rare Neurological Diseases Centre Neurology & Neurophysiopathology Unit, ASO San Camillo-Forlanini Hospital of Rome, Rome, Italy, [8]Section of Neuropathology, Neurological and Movement Sciences, University of Verona, Verona, Italy and [9]CNR Institute of Neurological Sciences, Mangone, Cosenza, Italy

*To whom correspondence should be addressed at: Department of Biology, University of Padova, via Ugo Bassi 58b, 35131 Padova, Italy. Tel: +39 049 8276226; Fax: +39 049 8276209; Email: giovanni.vazza@unipd.it

Abstract

Distal hereditary motor neuropathies (dHMNs) are clinically and genetically heterogeneous neurological conditions characterized by degeneration of the lower motor neurons. So far, 18 dHMN genes have been identified, however, about 80% of dHMN cases remain without a molecular diagnosis. By a combination of autozygosity mapping, identity-by-descent segment detection and whole-exome sequencing approaches, we identified two novel homozygous mutations in the *SIGMAR1* gene (p.E138Q and p.E150K) in two distinct Italian families affected by an autosomal recessive form of HMN. Functional analyses in several neuronal cell lines strongly support the pathogenicity of the mutations and provide insights into the underlying pathomechanisms involving the regulation of ER-mitochondria tethering, Ca^{2+} homeostasis and autophagy. Indeed, *in vitro*, both mutations reduce cell viability, the formation of abnormal protein aggregates preventing the correct targeting of sigma-1R protein to the mitochondria-associated ER membrane (MAM) and thus impinging on the global Ca^{2+} signalling. Our data definitively demonstrate the involvement of *SIGMAR1* in motor neuron maintenance and survival by correlating, for the first time in the Caucasian population, mutations in this gene to distal motor dysfunction and highlight the chaperone activity of sigma-1R at the MAM as a critical aspect in dHMN pathology.

[†]The authors wish to be known that the first two authors (EG and GP) should be regarded as joint First Authors.
Received: May 27, 2016. **Revised:** June 29, 2016. **Accepted:** June 30, 2016

Introduction

Distal hereditary motor neuropathies (dHMNs), also called distal spinal muscular atrophy (distal SMA), represent a group of progressive neurological diseases caused by degeneration of lower motor neurons with secondary distal muscle weakness and atrophy. Unlike hereditary motor and sensory neuropathy (HMSN), also known as Charcot-Marie-Tooth disease (CMT), sensory abnormalities are absent in dHMN or represent a minor component of the disease (1).

Genetically, dHMN is a heterogeneous condition inherited as an autosomal dominant, autosomal recessive or X-linked trait. Over the last 10 years, mutations in 18 genes (*HSPB1, HSPB8, BSCL2, IGHMBP2, SETX, GARS, DYNC1H1, DCTN1, ATP7A, TRPV4, SLC5A7, HSPB3, REEP1, HSJ1, BICD2, MYH14, AARS* and *FBXO38*) have been associated to dHMN (2,3). These genes encode proteins implicated in different cellular processes such as protein folding and quality control, RNA processing, axonal trafficking and ion channel function supporting that multiple pathogenic mechanisms may underlie the degeneration of motor neurons in dHMN. Despite these advances in gene discovery, further heterogeneity is expected in dHMN as mutations in the known genes account for only about 20% of dHMN patients (4). Furthermore, five additional chromosomal loci without identified disease genes have already been reported both for dominant (4q34-q35, 7q34-q36 and 2q14) and recessive dHMN forms (9p21.1-p12 and 11q13) (4). Recently, a mutation in the *SIGMAR1* gene has been reported in a consanguineous Chinese family with an autosomal recessive form of dHMN (5).

In this study, we combined whole-genome mapping and exome sequencing approaches to identify the gene responsible for a recessive form of dHMN clinically characterized in two Italian families.

Results

Clinical findings

Family 1 came from a small village of Southern Italy and pedigree reconstruction highlighted a consanguineous relationship between the parents of patient III-4 (first cousins), thus corroborating the recessive inheritance of the disease. On the contrary, no documented relationship was identified for parents of III-1 although all their ancestors came from the same village over four generations (Fig. 1A).

The proband (III-1), a 27 year-old female, displayed difficulties of gait since school age presenting recurrent sprains of the ankles and falls while running. At age 19 years, examination disclosed: bilateral pes cavus and claw hands; bilateral wasting of peroneal and sural muscles and of first interosseus, thenar and hypothenar muscles; stepping gait, impossible on heels and tips. Distal moderate-to-severe weakness was symmetrically present in the four limbs: according to the Medical Research Council (MRC) scale, strength was as follows: toe and ankle dorsiflexion = 0/5, plantar flexion = 2/5, intrinsic hand muscles = 3/5, the strength was normal in the remaining muscular districts. All modalities of sensation were preserved. Cranial nerves, bulbar and cerebellar functions were normal. Cognitive deficit was not detected. Deep tendon reflexes were absent in the distal lower limbs and brisk in the proximal lower and upper limbs; superficial reflexes were normal. Electromyography (EMG) disclosed diffuse signs of chronic denervation in the distal muscles of the four limbs. In nerve conduction studies, compound muscle action potential (CMAP) was unevokable in the lower limbs and markedly reduced (with conserved motor nerve conduction velocities) in the upper limbs; sensory nerve conduction studies were normal in lower (sural) and upper limbs (median and ulnar) nerves. Brain and spine magnetic resonance imaging (MRI), brainstem auditory, somatosensory and visual evoked potentials were normal. No clinical signs of dHMN were observed in the parents and in the two proband's siblings. The second affected subject (III-4) was referred to have clinical features similar to the proband, unfortunately she and her family refused to participate in the study.

The proband of the second family (II-2), aged 27 years at the first visit, reported ambulatory difficulties from the infancy and poor performance in physical activities during the school. The symptoms progressed very slowly in the following years, with walking impairment due to ankle distortions and difficulty in fine hand movements. Neurological examination revealed stepping gait and moderate muscle weakness and wasting in lower and upper limbs, more distal than proximal, with the following MRC strength scores: toe and ankle dorsiflexion = 2/5, plantar flexion = 2/5, intrinsic hand muscles = 2/5, wrist extension/flexion 3/5, weakness was absent at other levels. There were bilateral pes cavus, Babinski sign and hyperactive deep tendon reflexes without spasticity signs. Sensory, cerebellar, cranial nerves and bulbar functions were normal as well as respiratory and cognitive functions. Upper and lower limbs ENG revealed diffuse and marked reduction in CMAP amplitude with slightly reduced conduction velocities and preserved sensory conduction. Motor nerve conduction blocks were absent. Upper and lower limbs EMG disclosed diffuse signs of chronic denervation in the hand, forearm and leg muscles with normal findings in proximal muscles. Brain and spine MRI, as well as brainstem auditory, somatosensory and visual evoked potentials were normal. The proband's brother (II-1) was seen at 35 years of age, complaining running difficulties and motor hand impairment from childhood; he exhibited similar clinical findings and a comparable slow progression from the onset of the first symptoms; both brothers are still ambulant and independent in daily living activities after 25 years by symptoms onset. An ENG/EMG study disclosed similar neurophysiological findings. On clinical examination, the mother and a healthy sister of the patients did not show any signs or symptoms of neurological deficits at the age of 59 and 39 years, respectively.

Molecular genetic studies

In order to identify the disease gene, a genome-wide homozygosity mapping was performed on the proband, her parents and the two healthy siblings of family 1. The analysis of over 160.000 high-quality SNP genotypes identified 11 candidate homozygous regions greater than 1Mb inherited by the proband and not shared by her healthy siblings III-2 and III-3. A genome-wide IBD segment detection analysis was then carried out on the apparently unrelated parents II-1 and II-2 in order to quantify their relatedness and to identify DNA segments inherited from a common ancestor. IBD analysis revealed a single shared region on chromosome 9p with a probability of being inherited from a distant ancestor close to 1 (Fig. 1B). The same IBD interval overlaps with one of the homozygous regions previously identified in the proband and haplotype reconstruction confirmed the co-segregation with the disease (Fig. 1A). Despite the small size of the family, the combination of homozygosity mapping and IBD analysis allowed to identify a single candidate locus of about 7.9 Mb (rs17775810; rs1022770) on chromosome 9p21.1-p13.2.

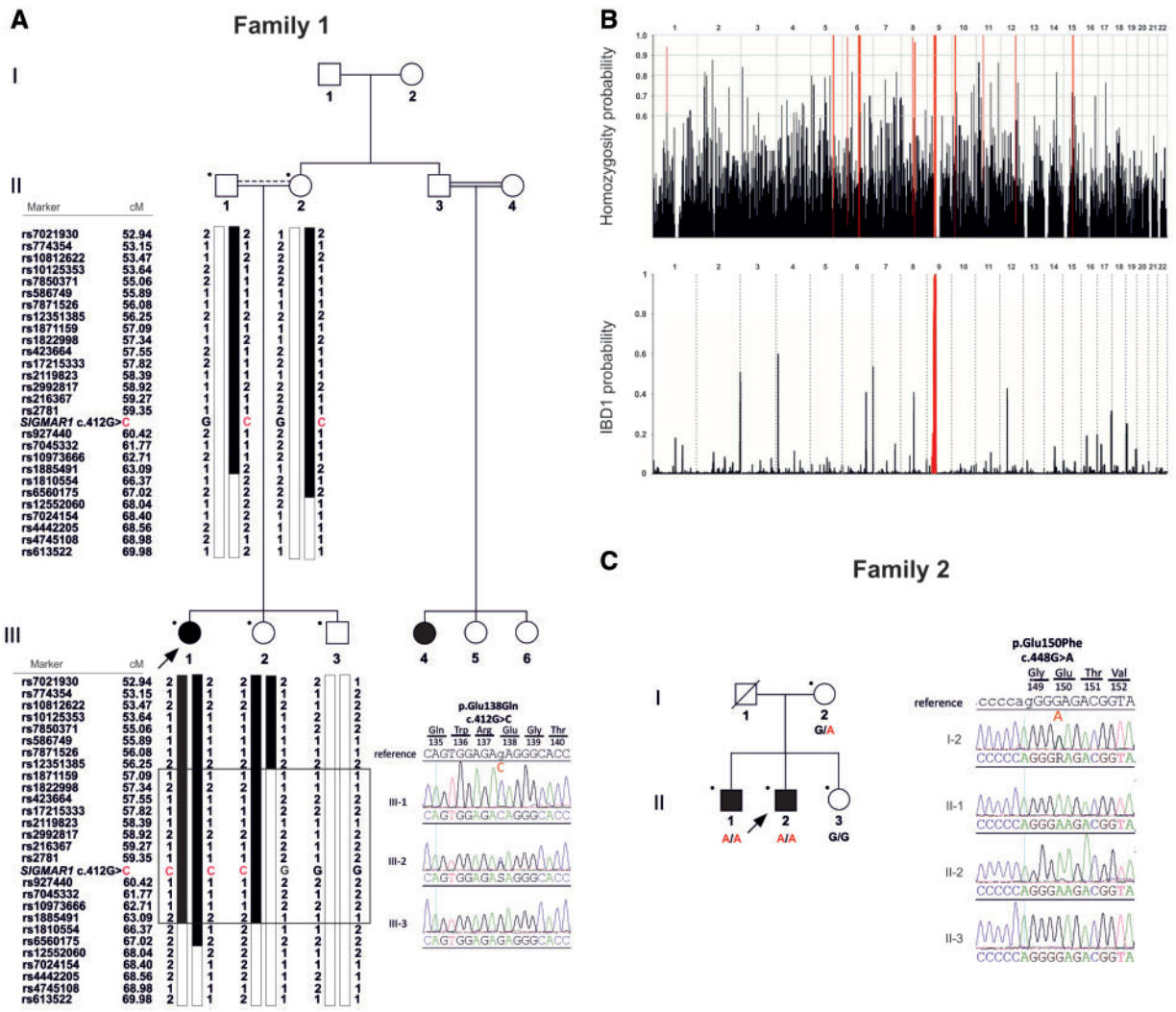

Figure 1. Pedigrees of the two Italian families with dHMN. (**A**) Pedigree of family 1 and haplotype reconstruction of the candidate region on chromosome 9p21.1-p13.2. The electropherogram with the novel c.412G > C mutation in the *SIGMAR1* gene and its segregation within the haplotypes are also reported in the panel. The proband is indicated by the arrow and dots indicate individuals taking part in this study. (**B**) Upper plot: Homozygosity mapping of the proband III-1 of family 1. The red lines indicate the 11 homozygous regions identified in the patient. Lower plot: Genome-wide IBD analysis of the proband's parents (II-1 and II-2) of family 1. A single peak with a maximum IBD1 probability of 0.98 was identified on chromosome 9p21.1-p13.2 (in red). (**C**) Pedigree of family 2, electropherogram showing the c.448G > A *SIGMAR1* mutation and its segregation in the family.

Whole-exome sequencing (mean coverage depth: 159X) was performed in the proband III-1 and no putative disease-causing variants were detected in any of the known genes associated with dHMN or with other related neuropathies. The analysis of WES variants in chr9p21.1-p13.2 identified a homozygous missense substitution (c.412G > C, p.E138Q, coverage depth: 149X, reads G = 0, C = 149) in the *SIGMAR1* gene (NM_005866). Sanger sequencing confirmed the presence of the homozygous variant exclusively in the patient III-1, whereas her parents (II-1 and II-2) and the unaffected sister III-2 were heterozygous (Fig. 1A).

No other putative disease-causing variants were identified in other genes in this region nor in other candidate genes in the remaining 10 homozygous regions. In order to confirm the involvement of *SIGMAR1* in the dHMN pathogenesis, a PCR-based mutation screening was performed in other 12 unrelated index patients diagnosed as having dHMN with a putative recessive inheritance.

In all these cases, mutations in the *HSPB1*, *HSPB8*, *BSCL2*, *IGHMBP2*, *GARS*, *HSPB3*, *HSJ1* genes, commonly involved in dHMN, were previously excluded by sanger sequencing.

A second homozygous missense variant (c.448G > A, p.E150K) was identified in one index case belonging to a small family with two affected brothers (Fig. 1C). The analysis of the other available family members confirmed the co-segregation of the homozygous *SIGMAR1* c.448G > A substitution with the disease.

Both c.412G > C and c.448G > A substitutions are neither reported in NHLBI Exome Variant Server, nor in other mutation databases including Leiden Open Variation Database, Human Gene Mutation Database and ClinVar (6–8). Only the c.448G > A is present in the ExAC database as it has been identified in heterozygosis in 1 out of 60315 subjects (allele frequency 0.000008). Moreover, they were not found in 200 control chromosomes from individuals of the same geographic area. Interestingly, *SIGMAR1* shows very high inter- and intra-species conservation; only 5 SNPs (MAF > 1%) are reported in its coding sequence according to dbSNP146. In addition, both the identified mutations occur in highly conserved nucleotides (PhyloP scores >5) and were predicted to be deleterious by several in silico analysis algorithms (Supplementary Material, Table S1).

SIGMAR1 encodes for the sigma non-opioid intracellular receptor 1 (sigma-1R), an integral membrane protein of the endoplasmic reticulum (ER) with chaperone activity implicated in many aspects of cellular homeostasis in the nervous system, including regulation of ion channels, calcium signalling (9), neurite outgrowth and autophagy (10).

The two identified amino acid changes occur in the C-terminus sigma-1R domain containing the ligand binding pocket (11) and with a putative chaperone function (12). Both mutations cause the replacement of a negatively charged residue with an uncharged (E138Q) or positively charged (E150K) residue.

Sigma-1R E138Q and E150K mutations affect neuronal cell survival

In order to identify the pathophysiological role of the two sigma-1R substitutions found in patients, we utilized three different neuronal cell systems, two human neuroblastoma cell lines, SH-SY5Y and SK-N-BE, and the murine motor neuron-like NSC-34 line. Given the relatively low level of endogenous sigma-1R protein in these cells, we overexpressed the two FLAG-tagged sigma-1R E138Q and E150K variants and compared the phenotype of transfected cells with that of cells overexpressing the WT sigma-1R.

We observed a protective effect of WT sigma-1R expression on cell survival after treatment of transfected cells with different ER stress inducers, namely H_2O_2 (1 mM) (13), MG132 (2.5 μM) and Thapsigargin (10 μM) (14). Interestingly, the expression of E138Q and E150K sigma-1R variants did not show this protection and, on the contrary, it further exacerbated the toxic effect of the treatments (Fig. 2A). To note, we observed a significant induction of cell death in cells expressing the sigma-1R E138Q and E150K mutations compared to cells expressing the WT protein, already in basal conditions (Fig. 2B).

E138Q and E150K mutations induce sigma-1R mislocalization out of the MAM

Sigma-1R protein localizes at specialized ER membrane regions in close contact to mitochondria, called mitochondria-associated ER membrane (MAM) (10) and actively participates to the Ca^{2+} transfer from ER to mitochondria during agonist-induced Ca^{2+} release in a variety of cellular models (9,14–16). This strategic localization ensures sigma-1R function as chaperone to IP3R channels at the ER-mitochondria interface and guarantees receptor activity and stability after ligand binding.

The immunofluorescence analysis in neuronal cells showed a cytoplasmic distribution of exogenous FLAG-tagged WT sigma-1R while both the E138Q and E150K mutants displayed an abnormal subcellular localization in both murine and human neuronal cells already in basal condition (Fig. 2C and Supplementary Material, Fig. S1A), which became even more striking in differentiated cells (Supplementary Material, Fig. S1B).

We then investigated the precise subcellular localization of overexpressed sigma-1R proteins confirming the ER membrane localization of WT sigma-1R, thus nicely reproducing that of the endogenous protein (10), as revealed by the colocalization with the ER marker calreticulin (Fig. 3A). Differently, both E138Q and E150K sigma-1R variants showed a dramatically reduced colocalization with calreticulin (Fig. 3A and B). This was also confirmed by the colocalization with another ER chaperone, GRP78/Bip (Supplementary Material, Fig. S2), which has been described to associate to sigma-1R and regulate its chaperone activity (10). We then analysed the localization of sigma-1R proteins at MAM, by staining transfected neuroblastoma cells with the mitochondrial marker TOM20. Here again, sigma-1R E138Q and E150K variants showed a significant reduction of colocalization with TOM20 compared to WT sigma-1R (Fig. 4). The same result was obtained by the analysis of colocalization between sigma-1R and the mitochondrial protein Mitofusin1 (not shown). This clearly points to a displacement of sigma-1R mutant proteins away from the MAM.

Impaired cellular Ca^{2+} handling in sigma-1R E138Q and E150K expressing cells

Considering the role of sigma-1R protein in assisting IP3Rs function during ER Ca^{2+} release in response to IP3-generating stimuli, and the mislocalization of the two sigma-1R mutants out of the MAM, we wondered whether they cause alteration in global Ca^{2+} homeostasis in neuronal cells. We then measured cytosolic and mitochondrial Ca^{2+} levels in resting condition and after Bradykinin (50 nM) stimulation in cells transfected with WT, E138Q and E150K sigma-1R using the ratiometric Fura-2 Ca^{2+} indicator or cotransfecting with the genetically encoded mitochondrial Ca^{2+} probe 4mt-GCaMP6f. As shown in Figure 5, both cytosolic Ca^{2+} increase and mitochondrial Ca^{2+} uptake were significantly reduced in cells expressing the two mutants compared to those expressing WT sigma-1R, despite both the cytosolic and mitochondrial resting Ca^{2+} were unaffected. We hypothesize that this is likely due to a loss of sigma-1R chaperone function to the IP3R channels rather than to a defect in the capacity of the ER to store Ca^{2+}, as suggested also in other cellular systems where the sigma-1R C-terminus domain is mutated (17).

Sigma-1R E138Q and E150K mutations induce p62 and LC3 aggregation

Considering: i) the position of the two identified mutations within the chaperone domain of sigma-1R; ii) the aggregate-like distribution (Fig. 2C and Supplementary Materials, Fig. S1A and B) and iii) the loss of cytoprotection (Fig. 2A and B) of the mutants, we investigated their effect on the cellular pathways involved in protein clearance and autophagy. To test this hypothesis, we analysed the expression and distribution of the two classical markers of autophagy in our cell models: p62 and LC3.

P62 lays at the crossroad of the two major proteolytic systems of the cell: the autophagy pathway and the proteasome-dependent protein degradation. Interestingly, we found that the expression of the mutated sigma-1R proteins induced a robust and significant increase of p62 reactive dots compared to WT sigma-1R in both human SH-SY5Y neuroblastoma and mouse NSC-34 cells (Fig. 6A and Supplementary Material, Fig. S3A).

LC3 is lipidated and redistributes to autophagosomes during autophagy induction appearing as fluorescent dots with punctate distribution inside the cell (18). The expression of both E138Q and E150K sigma-1R mutants correlated with a significant increase of LC3 positive autophagosomes (Fig. 6B). However, no significant colocalization between sigma-1R and p62 or LC3 was observed. We also investigated the distribution of another stress-activated chaperone involved in protein aggregate clearance, the heat shock protein HSP70 (19,20). HSP70 is found diffused in the cytoplasm in control mouse NSC-34 cells and in WT sigma-1R transfected cells and it did not

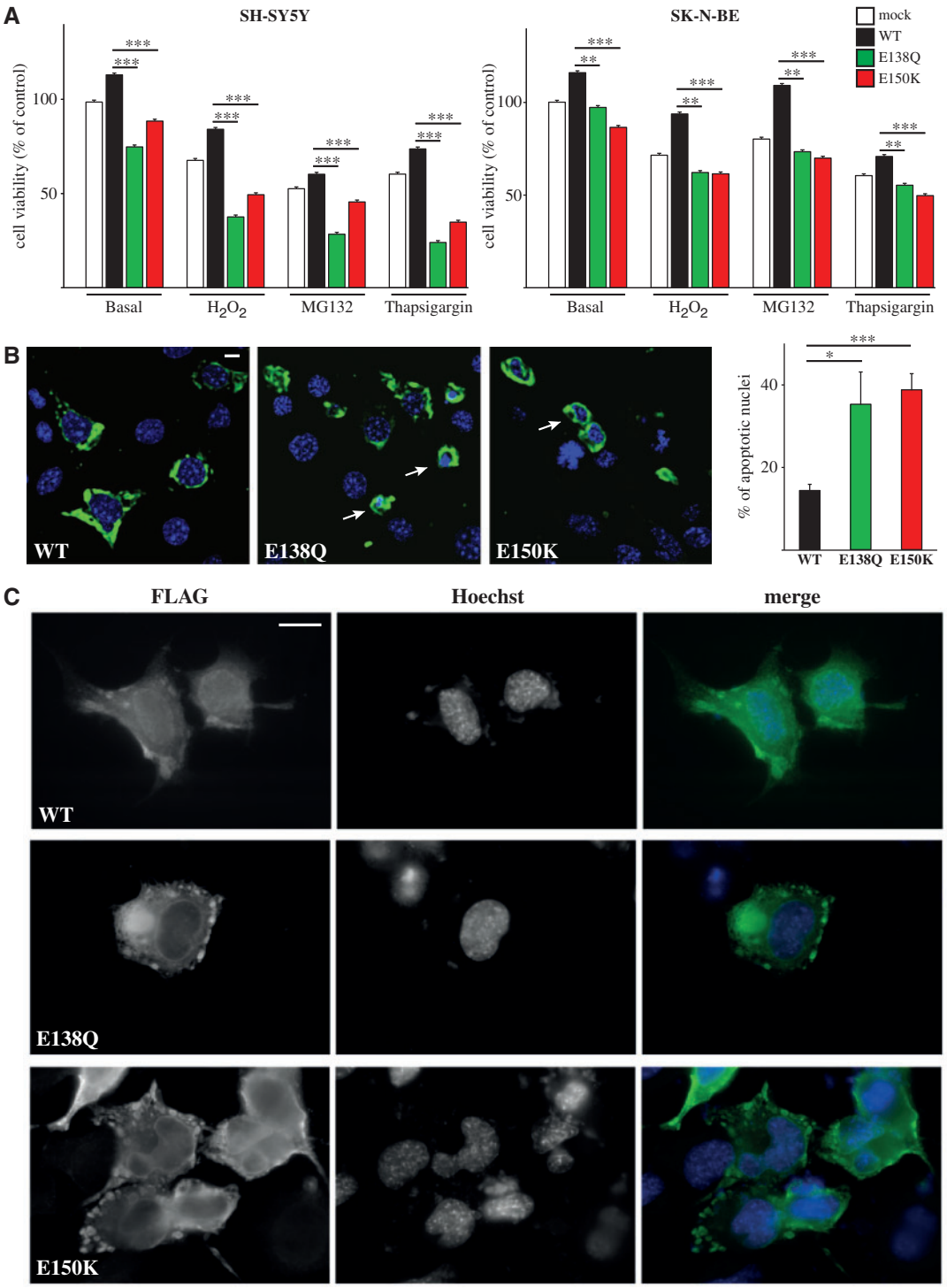

Figure 2. The expression of mutated sigma-1R proteins induces aggregate-like structures and increased cell death in neuronal cell cultures. (**A**) Measurements of cell viability by MTS assay of human SH-SY5Y (left) and SK-N-BE (right) neuroblastoma cells transfected with empty vector (mock) or plasmids coding for WT, E138Q and E150K FLAG-tagged sigma-1R and treated with H_2O_2 (1 mM), MG132 (2.5 μM) and Thapsigargin (10 μM) for 24 hours or not treated (Basal), as indicated. Cell viability is expressed as percentage of the untreated empty vector transfected cells. Data are presented as mean ± standard error from three independent experiments and a total of 30 replicates each condition. $^{**}P < 0.01$; $^{***}P < 0.001$. (**B**) The nuclear morphology of SH-SY5Y neuroblastoma cells transfected with FLAG-tagged WT, E138Q and E150K sigma-1R plasmids and immunostained with anti-FLAG antibodies, was assessed by Hoechst staining. The scale bar represents 10 μm. The graph on the right represents the quantification of apoptotic cells, expressed as the percentage of transfected cells displaying pyknotic condensed nuclei over the total number of FLAG-positive cells. $^{*}P < 0.05$; $^{***}P < 0.001$. (**C**) Representative images of mouse NSC-34 motoneuronal cells transfected and treated as in (B). The scale bar represents 10 μm.

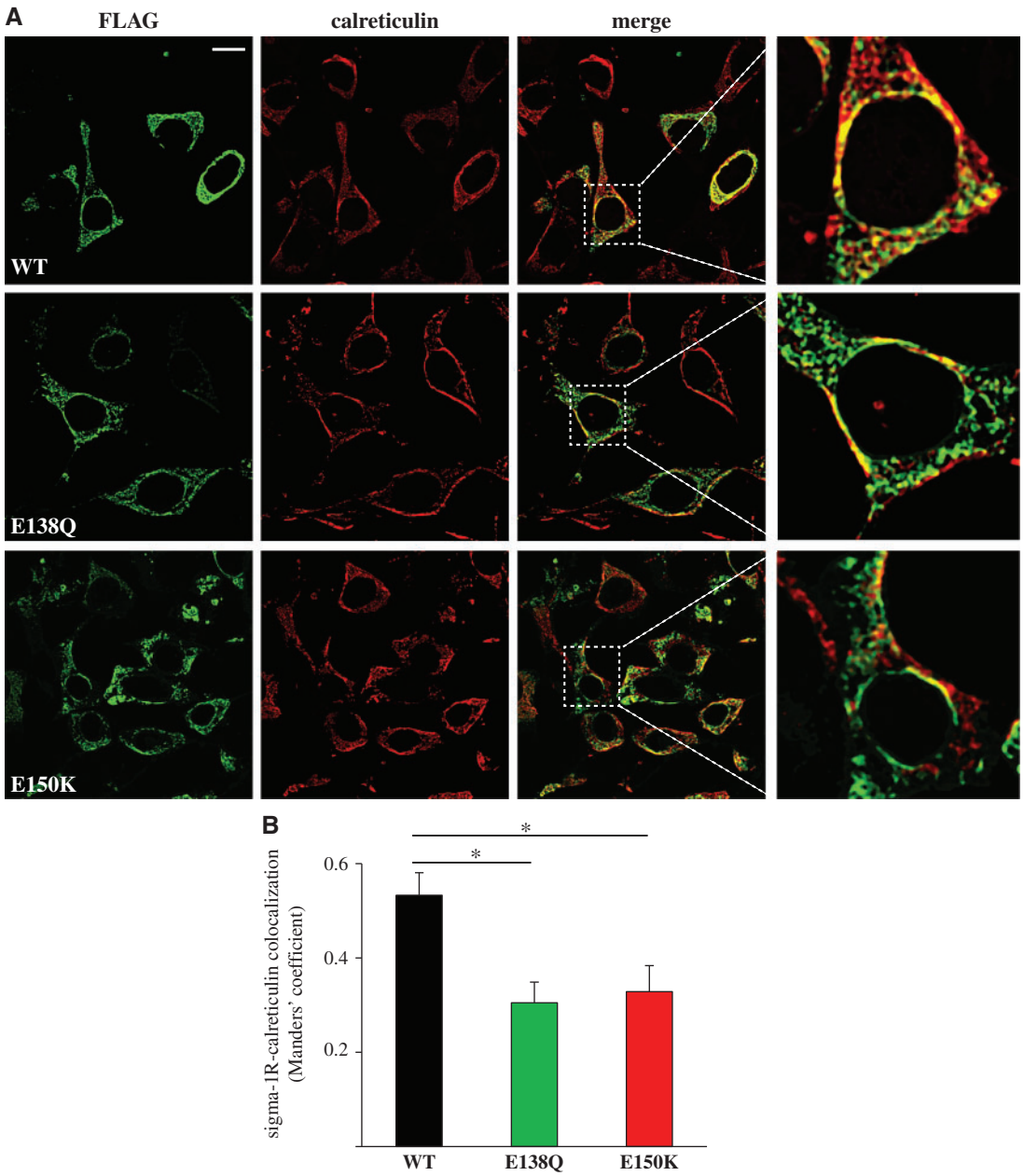

Figure 3. Sigma-1R mutants display a reduced colocalization with the ER marker calreticulin. (**A**) Representative images of human SH-SY5Y neuroblastoma cells transfected with WT, E138Q and E150K FLAG-tagged sigma-1R and immunostained with anti-FLAG (green) and anti-calreticulin (red) antibodies. The merge of the two stainings and a higher magnification of a representative cell are also shown on the right. The scale bar represents 10 μm. (**B**) Quantification of the Manders' coefficient (fraction of sigma-1R colocalizing with calreticulin), calculated on z-stack reconstructions of at least 60 confocal images each condition. Data are presented as mean ± standard error from three independent experiments. *$P < 0.05$.

colocalize with sigma-1R (Supplementary Material, Fig. S3B). Notably, the expression of sigma-1R patient mutations induced an overall increase of HSP70 positivity and an accumulation of HSP70 signal in punctate structures that were positive for sigma-1R. Unfortunately, the small percentage of transfected cells we recovered (Supplementary Material, Fig. S1C), prevented us to perform quantitative analysis of the HSP70 amount in the whole cell population extract.

Taken together, our observations indicate an induction of autophagosome formation following the expression of the two sigma-1R mutations. However, the mutated proteins seem not to be targeted for autophagic degradation, thus suggesting that their accumulation in aggregate-like structures precede recognition by the autophagy machinery or, alternatively, that they have already overwhelmed this degradation pathway.

Discussion

By using a combination of homozygosity mapping, IBD analysis and whole-exome sequencing approaches, we identified two homozygous missense *SIGMAR1* mutations in two Italian families affected by a distal form of autosomal recessive hereditary motor neuropathy (dHMN).

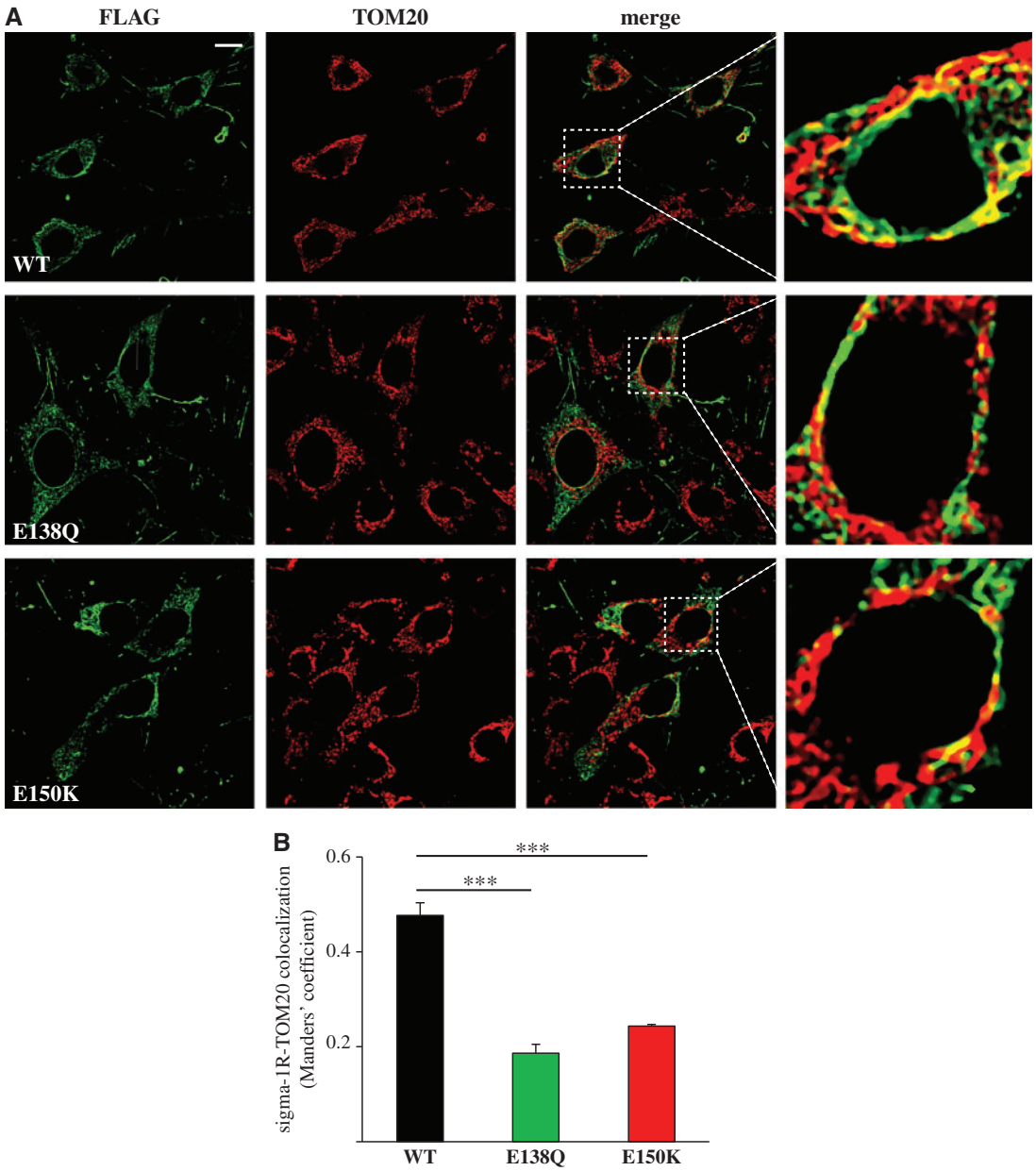

Figure 4. Sigma-1R mutants mislocalize out of MAM. (**A**) Representative images of human SH-SY5Y neuroblastoma cells transfected with WT, E138Q and E150K FLAG-tagged sigma-1R and immunostained with anti-FLAG (green) and anti-TOM20 (red) antibodies. The merge of the two stainings and a higher magnification of a representative cell are also shown on the right. The scale bar represents 10 μm. (**B**) Quantification of the Manders' coefficient (fraction of sigma-1R colocalizing with TOM20), calculated on z-stack reconstructions of at least 60 confocal images each condition. Data are presented as mean ± standard error from three independent experiments. ***$P < 0.001$.

In 2011, a *SIGMAR1* homozygous mutation has been identified in a consanguineous Saudi Arabian family affected by a form of juvenile amyotrophic lateral sclerosis (21). This form has been classified as jALS16, however, no other mutations have been identified in extensive molecular screenings of ALS and frontotemporal lobar degeneration patients (22,23). More recently, a 3′-UTR *SIGMAR1* nucleotide variation (c.672*31A > G) has been reported as candidate in two Pakistani brothers with ALS (24), however, from recent polymorphism databases, the mutated allele seems to be very common in several populations (SNP rs4879809, G-allele frequency >0.95). A *SIGMAR1* splice site mutation has been also identified in a single Chinese consanguineous family with a form of dHMN (5) but the small family size may leave uncertainty about the association with the phenotype.

Despite these reports, the association of *SIGMAR1* with human diseases remains still controversial as *SIGMAR1* mutations have been identified only in small and isolated non-Caucasian families, with limited genetic and functional supporting data and never confirmed in other patients.

In this context, our study identifies, for the first time, *SIGMAR1* mutations in Caucasian families with dHMN and definitively demonstrates the role of *SIGMAR1* in the pathogenesis of a heterogeneous group of motor neuropathies mainly characterized by distal motor dysfunction (dHMN). This gene should be thus screened in patients with such phenotype worldwide,

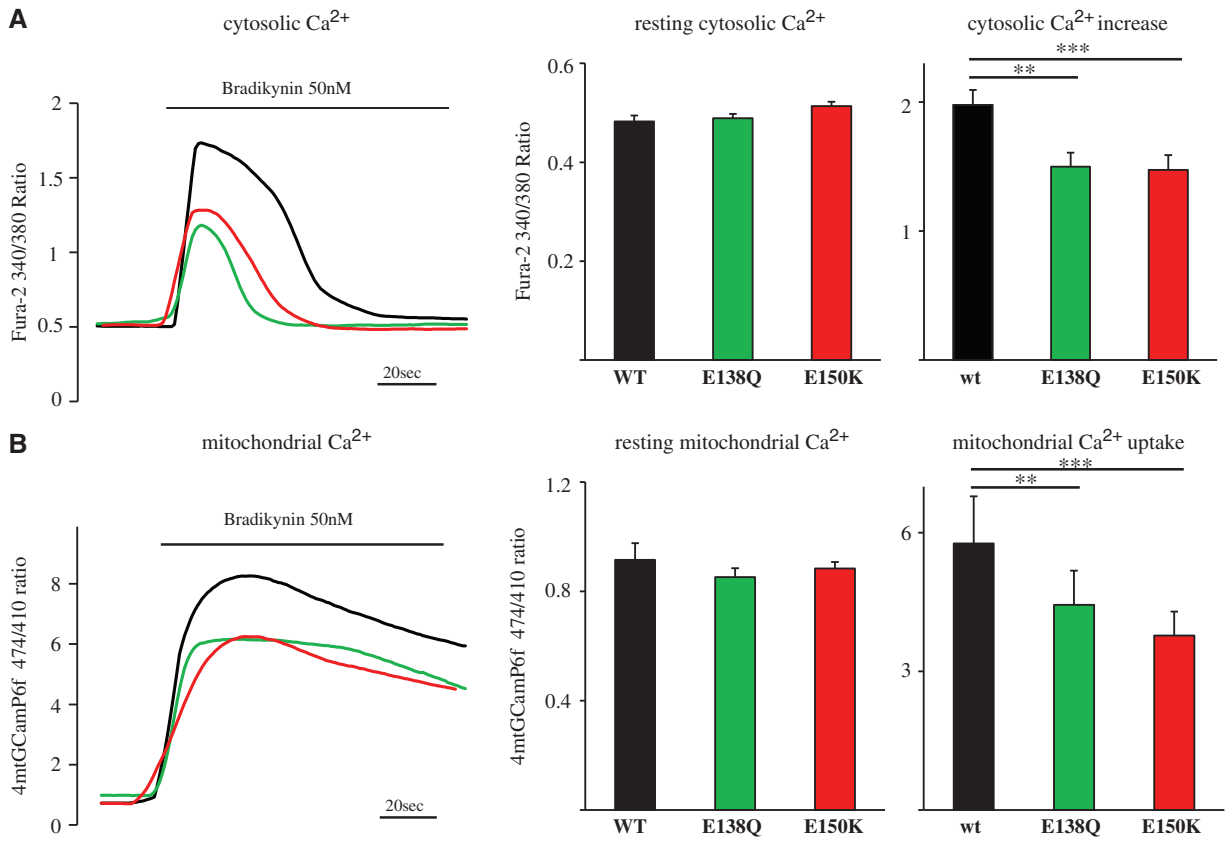

Figure 5. The expression of sigma-1R mutants impairs global Ca^{2+} signalling in human neuroblastoma cells. (**A**) Representative traces and average measures of cytosolic Ca^{2+} level in human SH-SY5Y neuroblastoma cells transfected with WT, E138Q and E150K sigma-1R and loaded with Fura-2 Ca^{2+} indicator, before (resting) and after (peak value) the addition of the IP3-generating agonist (Bradykinin 50 nM). (**B**) Representative traces and average measures of mitochondrial Ca^{2+} level in human SH-SY5Y neuroblastoma cells cotransfected with 4mt-GCaMP6f and WT, E138Q or E150K sigma-1R, and treated as in (A). Data are presented as mean ± standard error from at least three independent experiments. $^{**}P < 0.01$; $^{***}P < 0.001$.

as mutations have been now documented in different ethnic populations. Phenotypically, the spectrum of *SIGMAR1* mutations manifestations is wide and includes ALS and distal spinal muscle atrophy with pyramidal signs, as reported in the present work and by Li *et al.* (5) (Table 1).

To note, *SIGMAR1* maps within the known recessive Jerash dHMN locus, identified in consanguineous families from the Jerash region of Jordan and still orphan of the disease-causing gene (OMIM: 605726) (25). The phenotype similarity of our families, the Chinese family and the Jordan ones, allows speculation on the involvement of *SIGMAR1* in the Jerash dHMN form (Table 1).

The genetic overlap between dHMN and ALS is not unusual; for instance, *SETX* mutations have been listed as a cause of both distal motor neuropathy with pyramidal features and the jALS-type 4 (26,27).

SIGMAR1 encodes for the sigma non-opioid intracellular receptor 1 (sigma-1R), a ubiquitously expressed integral membrane protein of the ER, mainly associated with the so called MAM (mitochondria-associated ER membrane), exerting regulatory actions on the UPR, calcium homeostasis through interaction with the IP3 receptors, apoptosis and neuroprotection (28). Sigma-1R has been demonstrated to regulate dendritic spine formation and dendrite arborization (29) and to play a cytoprotective role after tissue injury as infarction and oxidative stress (13). Changes in *SIGMAR1* expression or function have been observed in several psychiatric and neurological disorders including depression, schizophrenia, stroke, drug addiction, age-related cognitive impairments and ALS (30,14).

This multifaceted but yet poorly understood functions of sigma-1R strongly complicate the dissection of the mechanisms through which its mutations lead to pathogenesis in dHMN. However, the results of our functional studies obtained from overexpression experiments, clearly showed that both mutations affect cell viability in human neuroblastoma cells. More interestingly, while the expression of WT sigma-1R is *per se* protective against oxidative and ER stress (Fig. 2A and 13), the E138Q and E150K sigma-1R mutants lack this cytoprotective function.

In addition to that, our immunofluorescence studies evidenced a significant mislocalization of mutated sigma-1R proteins out of MAM (Fig. 4) and a reduction of the total MAM number in cells overexpressing the E138Q and E150K sigma-1R (not shown). Despite further studies are needed to definitively clarify the issue, it is conceivable that these amino acid substitutions may affect the role of sigma-1R on the establishment and maintenance of functional MAM in human neuroblastoma cells, similar to what described in motor neurons from *SIGMAR1*$^{-/-}$ mice (9). As a consequence, the global cellular Ca^{2+} signalling in cells expressing the two sigma-1R variants is significantly impaired, as revealed by the markedly decrease in the mitochondrial Ca^{2+} uptake (Fig. 5). This is expected, given the reduced tethering between the ER Ca^{2+} store and mitochondria in these conditions, and it is in line with the published data

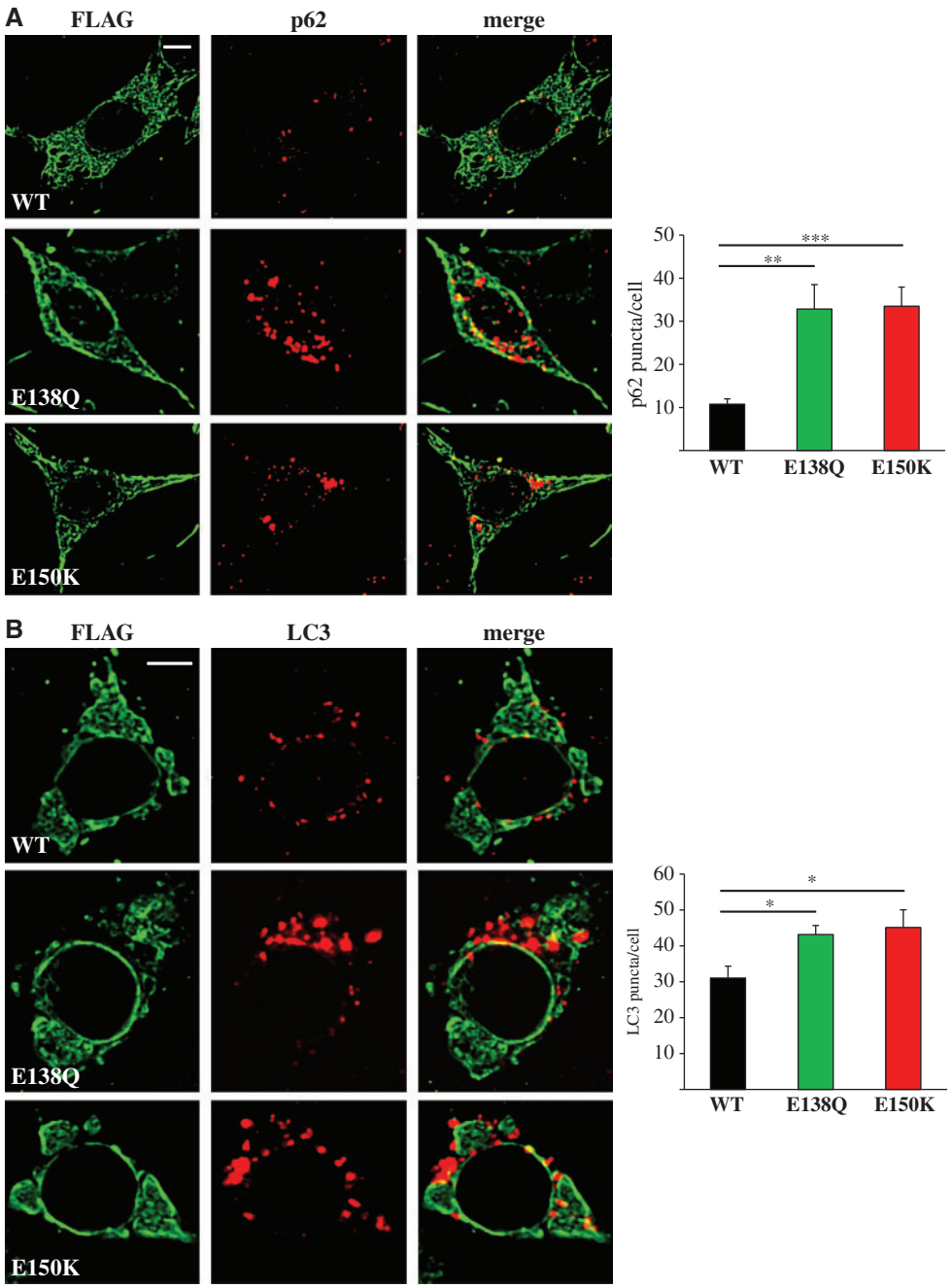

Figure 6. The expression of mutated sigma-1R proteins induces p62 and LC3-positive autophagosome formation. (**A**) Representative images of human SH-SY5Y cells transfected with FLAG-tagged WT, E138Q and E150K sigma-1R and immunostained with anti-FLAG and anti-p62 (A) or anti-LC3 (**B**) antibodies. The scale bar represents 10 μm. The graphs on the right represent the quantification of p62 (A) and LC3-positive (B) dots identified as autophagosomes. Data are presented as mean ± standard error from two independent experiments. At least 40 cells were measured each condition. *$P < 0.05$; **$P < 0.01$; ***$P < 0.001$.

from *SIGMAR1* loss of function models (10,15). Interestingly, the regulation of ER Ca^{2+} release has a major role in the survival of neuronal cells, as its alteration has been recently seen to significantly contribute to degeneration of spinal axons (31).

To note, despite the fact that silencing of *SIGMAR1* is reported to increase cytosolic Ca^{2+} level both in resting conditions (9,10) and after stimulation (14,15) in different cellular models, our findings indicated that E138Q and E150K sigma-1R mutations selectively reduced the cytosolic Ca^{2+} transients after agonist stimulation, with no alteration of the resting cytosolic Ca^{2+} level. Several explanations could account for this apparent discrepancy: i) different cell types could manifest different sensitivity of Ca^{2+} responses to stress conditions (14,32,33); ii) the effect of mutated unfunctional proteins could be different from that of the complete lack of the protein, especially in the case of molecules with multiple binding partners as the sigma-1R chaperone; iii) an increased cytosolic Ca^{2+} level has been also reported as consequence of WT sigma-1R overexpression or sigma-1R agonist stimulation (17,34), as we found in neuroblastoma cells (not shown). Thus, the reduction of cytosolic Ca^{2+} peak observed in E138Q and E150K expressing cell would result from to the lack of the sigma-1R-mediated effect.

Table 1. Main clinical features of patients analysed in this study together with clinical information reported for Jerash dHMN, jALS16 and the Chinese family

	Family 1 dHMN (this study)	Family 2 dHMN (this study)	Jerash type dHMN(25)	Arabian Family jALS16(21)	Chinese Family dHMN(5)
Distal muscle wasting and weakness of the four limbs	+	+	+	+	+
Brisk deep tendon reflexes	+	+	+	+	+
Babinski sign	–	+	+	n.a.	+/–
Spasticity	–	–	–	+	–
Proximal muscle wastingand weakness	–	–	–	+	–
Bulbar signs	–	–	–	–	n.a
Respiratory signs	–	–	–	–	n.a

In light of the emerging impact of protein quality control in neurodegenerative diseases, we demonstrated that the sigma-1R mutations identified in dHMN patients are also relevant to the more general protein folding and homeostasis. Indeed, both variants displayed an altered distribution and tended to form aggregate-like structures. A similar aberrant sigma-1R distribution was also found in cells expressing the E102Q mutation associated with jALS16 (21) and in the splice variant associated with dHMN (5). Immunofluorescence analysis of overexpressing cells revealed that the E138Q and E150K mutations induces p62 and LC3 accumulation in the cytoplasm of cells from both human and mouse origin, indicating the involvement of the autophagy pathway. In addition, sigma-1R mutations induced the up-regulation of the stress response protein HSP70.

Notably, the E150K and to a lesser extent the E138Q mutations induced HSP70 but not p62 colocalization with sigma-1R aggregates, similarly to what was reported in motor neurons of ALS patients carrying mutations in the *VAPB* gene (14). This suggests the involvement of the Ubiquitin-proteasome pathway in the degradation of mutated sigma-1R and points to a similar pathogeneic mechanism for *SIGMAR1* and *VAPB* mutations. However, the correlation between the expression of sigma-1R variants and the increase of LC3 dots indicated that the autophagy pathway is also involved in our model. Indeed, the reduction of sigma-1R function has been recently associated with induction of autophagy in a breast cancer model (35) and in retinal cells (36), further supporting the hypothesis that the identified mutations lead to the loss of *SIGMAR1* function. Despite the induction of autophagosome formation, the two sigma-1R mutants did not colocalize with autophagosome-associated p62 and LC3 (Fig. 6A and B and Supplementary Material, Fig. S3A), indicating that these mutated proteins escape the degradation pathway or, alternatively, that this pathway is somehow impaired. Additional functional studies are needed in the future to clarify if the described mutations cause stalling of the autophagy flux and how this contributes to the pathomechanism of dHMN. To note, the formation of protein aggregates and the impairment of the autophagy pathway have also been observed for mutated HspB8, a small heat-shock protein responsible for the dHMN type II (37).

Considering the recessive mode of the disease inheritance and our data, dHMN pathology is likely due to a loss of functional sigma-1R in motor neurons. Despite this, a gain-of-function mechanism cannot be definitively excluded as the abnormal sigma-1R protein accumulation might compromise the protein clearance and autophagy pathways, which are crucial for neuronal survival (38). However, we cannot rule out that this effect may become overt due to the expression level of sigma-1R protein in our experimental model. Further investigation, especially in the context of patient-derived cells, would be thus desirable to definitively unravel the complex signalling pathway triggered by *SIGMAR1* mutations and solve the issue of their loss- or gain-of-function mechanism in the dHMN pathogenesis.

Concluding, our findings represent a step forward the dissection of these mechanisms providing insights into this neurodegenerative disorder and hopefully leading to the identification of potential therapeutic strategies based on the use of sigma-1R-specific drugs (39).

Materials and Methods

Genome-wide SNP genotyping and analysis

The DNA of the available family members was extracted from whole blood by following the standard phenol/chloroform method. Written informed consents were obtained from all the participants in this study.

One affected and four unaffected members of family 1 were genotyped using the Mendel Nsp 250K Genechip (Affymetrix) according to the manufacturer's protocol. Quality controls were carried out in order to filter out SNPs with Mendelian errors and high genotyping failure. HomozygosityMapper (40) software was used to identify homozygous chromosomal regions in the proband of family 1 (III-1) and not present in the two healthy brothers (III-2, III-3). HomozygosityMapper calculates a homozygosity score for each marker based on the length of the homozygous blocks. Parameters for defining a homozygous stretch are optimized for the SNP array; a minimum cut-off size of 1Mb was used to reduce the influence of non-informative segments.

Identity-by-descent (IBD) chromosomal regions were searched by RELATE, a tool for detecting pairwise IBD from unphased haplotype data. (41) To prevent bias due to linkage disequilibrium (LD), the genome-wide SNP dataset was pruned to roughly 64.000 SNPs in low LD.

Whole-exome sequencing and Sanger sequencing

High-coverage whole-exome sequencing was performed for the proband III-1 of family 1 at BGI. Agilent SureSelect Human All Exon v4 kit for the targeted enrichment and the Illumina Hiseq2000 platform for the sequencing were used. End-paired reads were aligned against the human reference sequence (hg19) with the SOAPaligner/SOAP2 program, and all sequence variants were called by SOAPsnp software. GATK and Copy Number Inference From Exome Reads (CoNIFER) software were used to detect small and large indels respectively. (42,43) Called variants were then searched in dbSNP146, 1000 Genomes, and ExAC repositories, to filter out common Single Nucleotide Polymorphisms (SNPs) with MAF $>$ 0.5%. Variants were then prioritized according

to the type of mutation (deletion/insertion > nonsense > missense), amino acid conservation, prediction of pathogenicity and relevance of the candidate gene to the disease. A nucleotide position was considered highly conserved whenever the relative PhiloP score was > 2. In silico variant effect predictions were performed by a majority vote across three independent algorithms: MutationTaster2 (44), CONDEL (45) and LRT (46).

Control DNA samples were tested for both mutations by direct sequencing on the 3100 ABI Prism Genetic Analyzer (Applied Biosystems, Foster City, CA, USA).

Cell cultures, transfection and viability studies

pcDNA3 vector coding for FLAG-tagged sigma-1R (NM_005866) was kindly provided by Dr. Changlong Hu (Shanghai) (47). The c.412G > C and c.448C > G mutations were introduced by site-directed mutagenesis in the *SIGMAR1* cDNA by using the primers 5'-CCTTCCACCAGTGGAGACAGGGCACCACCAAAAGTGAGG-3' and 5'-GGTCTTCTACCCAGGGAAGACGGTAGTACACGGGCC-3', respectively. The cell culture, cell transfection and cell viability measurement procedures can be found as Supplementary Material.

Immunofluorescence analysis

Cells were seeded on 13 mm coverslips and the day after transfected with Lipofectamine2000 reagent (Thermofisher) following manufacturer's instructions, fixed after 48 h and processed for immunofluorescence as previously described. (48,49) For a detailed procedure, see Supplementary Material.

Cytosolic Ca^{2+} measurements

Cells were loaded with 2 μM Fura-2-AM (Life Technologies) diluted in Krebs-Ringer modified buffer containing 0.02% pluronic acid and 250 μM sulfinpyrazone for 20 min at 37 °C and then washed with Krebs-Ringer modified buffer. In all the experiments, images were acquired every 1s with a Zeiss Axiovert 200 microscope equipped with a Fluar 40x/1.3 N.A. oil immersion objective (Zeiss) and a high-sensitivity 16-bit Evolve 512 Delta EMCCD (Photometrics). Exposure time was set to 300 ms. Excitation was performed with a DeltaRAM V highspeed monochromator (Photon Technology International) equipped with a 75 W xenon arc lamp. The system is controlled by MetaMorph 7.5 (Molecular Devices) and was assembled by Crisel Instruments. Images were collected by alternatively exciting the fluorophore at 340 and 380 nm and fluorescence emission recorded through a 515/30 nm band-pass filter (Semrock). Changes in fluorescence (340/380 nm ratio) were expressed as $\Delta R/R0$, where $\Delta R = (R-R0)$, R is the ratio at time t and R0 is the ratio at the beginning of the experiment.

Mitochondrial Ca^{2+} measurements

Mitochondrial Ca^{2+} measurements were performed in human SH-SY5Y cells transfected with the mitochondrial-targeted GCaMP6m (4mt-GCaMP6f) coding plasmid (Addgene) and assayed 48 h after. 4mt-GCaMP6f was alternately excited at 474 and 410 nm and images were collected through a 535/20 band-filter (Semrock) (50). For all the experiments, exposure time was set to 200 ms and images were acquired every 1s. Changes in mitochondrial Ca^{2+} levels were expressed as $\Delta R/R0$, where $\Delta R = (R-R0)$, R is the 474/410 nm fluorescence ratio at time t and R0 is the ratio at the beginning of the experiment. Analysis was performed with the Fiji distribution of ImageJ (51). Images were background corrected frame by frame by subtracting the mean pixel value of a cell-free region of interest.

Supplementary Material

Supplementary Material is available at HMG Online.

Acknowledgements

We are grateful to the members of the family who participated in the study. We also thank Angela Rosini for her secretarial help.

Conflict of Interest statement. None declared.

Funding

This work was supported by the Fondazione Telethon-Italy (grant no. GEP12083 to VG), the Italian Ministry of Education, University and Research (FIRB no. RBAP11X42L_004) and the European Research Council (ERC grant mitoCalcium no. 294777 to RR).

References

1. Vallat, J.M., Mathis, S. and Funalot, B. (2013) The various Charcot-Marie-Tooth diseases. *Curr. Opin. Neurol.*, **26**, 473–480.
2. Rossor, A.M., Polke, J.M., Houlden, H. and Reilly, M.M. (2013) Clinical implications of genetic advances in Charcot-Marie-Tooth disease. *Nat. Rev. Neurol.*, **9**, 562–571.
3. Sumner, C.J., d'Ydewalle, C., Wooley, J., Fawcett, K.A., Hernandez, D., Gardiner, A.R., Kalmar, B., Baloh, R.H., Gonzalez, M., Zuchner, S., *et al.* (2013) A dominant mutation in FBXO38 causes distal spinal muscular atrophy with calf predominance. *Am. J. Hum. Genet.*, **93**, 976–983.
4. Rossor, A.M., Kalmar, B., Greensmith, L. and Reilly, M.M. (2012) The distal hereditary motor neuropathies. *J. Neurol. Neurosurg. Psychiatry*, **83**, 6–14.
5. Li, X., Hu, Z., Liu, L., Xie, Y., Zhan, Y., Zi, X., Wang, J., Wu, L., Xia, K., Tang, B., *et al.* (2015) A SIGMAR1 splice-site mutation causes distal hereditary motor neuropathy. *Neurology*, **84**, 2430–2437.
6. Fokkema, I.F., Taschner, P.E., Schaafsma, G.C., Celli, J., Laros, J.F. and den Dunnen, J.T. (2011) LOVD v.2.0: the next generation in gene variant databases. *Hum. Mutat.*, **32**, 557–563.
7. Landrum, M.J., Lee, J.M., Riley, G.R., Jang, W., Rubinstein, W.S., Church, D.M. and Maglott, D.R. (2014) ClinVar: public archive of relationships among sequence variation and human phenotype. *Nucleic Acids Res.*, **42**, D980–D985.
8. Stenson, P.D., Ball, E.V., Mort, M., Phillips, A.D., Shaw, K. and Cooper, D.N. (2012) The Human Gene Mutation Database (HGMD) and its exploitation in the fields of personalized genomics and molecular evolution. *Curr. Protoc. Bioinformatics*, Chapter 1, Unit1 13.
9. Bernard-Marissal, N., Medard, J.J., Azzedine, H. and Chrast, R. (2015) Dysfunction in endoplasmic reticulum-mitochondria crosstalk underlies SIGMAR1 loss of function mediated motor neuron degeneration. *Brain*, **138**, 875–890.

10. Hayashi, T. and Su, T.P. (2007) Sigma-1 receptor chaperones at the ER-mitochondrion interface regulate Ca(2+) signaling and cell survival. *Cell*, **131**, 596–610.
11. Schmidt, H.R., Zheng, S., Gurpinar, E., Koehl, A., Manglik, A. and Kruse, A.C. (2016) Crystal structure of the human sigma1 receptor. *Nature*, **532**, 527–530.
12. Ortega-Roldan, J.L., Ossa, F. and Schnell, J.R. (2013) Characterization of the human sigma-1 receptor chaperone domain structure and binding immunoglobulin protein (BiP) interactions. *J. Biol. Chem.*, **288**, 21448–21457.
13. Wang, L.X., Eldred, J.A., Sidaway, P., Sanderson, J., Smith, A.J.O., Bowater, R.P., Reddan, J.R. and Wormstone, I.M. (2012) Sigma 1 receptor stimulation protects against oxidative damage through suppression of the ER stress responses in the human lens. *Mec. Ageing Dev.*, **133**, 665–674.
14. Prause, J., Goswami, A., Katona, I., Roos, A., Schnizler, M., Bushuven, E., Dreier, A., Buchkremer, S., Johann, S., Beyer, C., *et al.* (2013) Altered localization, abnormal modification and loss of function of Sigma receptor-1 in amyotrophic lateral sclerosis. *Hum. Mol. Genet.*, **22**, 1581–1600.
15. Shioda, N., Ishikawa, K., Tagashira, H., Ishizuka, T., Yawo, H. and Fukunaga, K. (2012) Expression of a truncated form of the endoplasmic reticulum chaperone protein, sigma1 receptor, promotes mitochondrial energy depletion and apoptosis. *J. Biol. Chem.*, **287**, 23318–23331.
16. Mori, T., Hayashi, T., Hayashi, E. and Su, T.P. (2013) Sigma-1 receptor chaperone at the ER-mitochondrion interface mediates the mitochondrion-ER-nucleus signaling for cellular survival. *PLoS One*, **8**, e76941.
17. Wu, Z. and Bowen, W.D. (2008) Role of sigma-1 receptor C-terminal segment in inositol 1,4,5-trisphosphate receptor activation: constitutive enhancement of calcium signaling in MCF-7 tumor cells. *J. Biol. Chem.*, **283**, 28198–28215.
18. Klionsky, D.J., Abdalla, F.C., Abeliovich, H., Abraham, R.T., Acevedo-Arozena, A., Adeli, K., Agholme, L., Agnello, M., Agostinis, P., Aguirre-Ghiso, J.A., *et al.* (2012) Guidelines for the use and interpretation of assays for monitoring autophagy. *Autophagy*, **8**, 445–544.
19. Mayer, M.P. and Bukau, B. (2005) Hsp70 chaperones: cellular functions and molecular mechanism. *Cell. Mol. Life Sci.*, **62**, 670–684.
20. Wong, E. and Cuervo, A.M. (2010) Integration of clearance mechanisms: the proteasome and autophagy. *Cold Spring Harb. Perspect. Biol.*, **2**, a006734.
21. Al-Saif, A., Al-Mohanna, F. and Bohlega, S. (2011) A mutation in sigma-1 receptor causes juvenile amyotrophic lateral sclerosis. *Ann. Neurol.*, **70**, 913–919.
22. Belzil, V.V., Daoud, H., Camu, W., Strong, M.J., Dion, P.A. and Rouleau, G.A. (2013) Genetic analysis of SIGMAR1 as a cause of familial ALS with dementia. *Eur. J. Hum. Genet.*, **21**, 237–239.
23. Kim, H.J., Kwon, M.J., Choi, W.J., Oh, K.W., Oh, S.I K., C.S., and Kim, S.H., (2014) Mutations in UBQLN2 and SIGMAR1 genes are rare in Korean patients with amyotrophic lateral sclerosis. *Neurobiol. Aging*, **35**, e19571958–e19571957.
24. Ullah, M.I., Ahmad, A., Raza, S.I., Amar, A., Ali, A., Bhatti, A., John, P., Mohyuddin, A., Ahmad, W. and Hassan, M.J. (2015) In silico analysis of SIGMAR1 variant (rs4879809) segregating in a consanguineous Pakistani family showing amyotrophic lateral sclerosis without frontotemporal lobar dementia. *Neurogenetics*, **16**, 299–306.
25. Christodoulou, K., Zamba, E., Tsingis, M., Mubaidin, A., Horani, K., Abu-Sheik, S., El-Khateeb, M., Kyriacou, K., Kyriakides, T., Al-Qudah, A.K., *et al.* (2000) A novel form of distal hereditary motor neuronopathy maps to chromosome 9p21.1-p12. *Ann. Neurol.*, **48**, 877–884.
26. Chen, Y.Z., Bennett, C.L., Huynh, H.M., Blair, I.P., Puls, I., Irobi, J., Dierick, I., Abel, A., Kennerson, M.L., Rabin, B.A., *et al.* (2004) DNA/RNA helicase gene mutations in a form of juvenile amyotrophic lateral sclerosis (ALS4). *Am. J. Hum. Genet.*, **74**, 1128–1135.
27. Hirano, M., Quinzii, C.M., Mitsumoto, H., Hays, A.P., Roberts, J.K., Richard, P. and Rowland, L.P. (2011) Senataxin mutations and amyotrophic lateral sclerosis. *Amyotroph. Lateral. Scler.*, **12**, 223–227.
28. Ruscher, K. and Wieloch, T. (2015) The involvement of the sigma-1 receptor in neurodegeneration and neurorestoration. *J. Pharmacol. Sci.*, **127**, 30–35.
29. Tsai, S.Y., Hayashi, T., Harvey, B.K., Wang, Y., Wu, W.W., Shen, R.F., Zhang, Y., Becker, K.G., Hoffer, B.J. and Su, T.P. (2009) Sigma-1 receptors regulate hippocampal dendritic spine formation via a free radical-sensitive mechanism involving Rac1xGTP pathway. *Proc. Natl. Acad. Sci. U S A*, **106**, 22468–22473.
30. Kourrich, S., Su, T.P., Fujimoto, M. and Bonci, A. (2012) The sigma-1 receptor: roles in neuronal plasticity and disease. *Trends Neurosci.*, **35**, 762–771.
31. Stirling, D.P., Cummins, K., Wayne Chen, S.R. and Stys, P. (2014) Axoplasmic reticulum Ca(2+) release causes secondary degeneration of spinal axons. *Ann. Neurol.*, **75**, 220–229.
32. Spruce, B.A., Campbell, L.A., McTavish, N., Cooper, M.A., Appleyard, M.V., O'Neill, M., Howie, J., Samson, J., Watt, S., Murray, K., *et al.* (2004) Small molecule antagonists of the sigma-1 receptor cause selective release of the death program in tumor and self-reliant cells and inhibit tumor growth in vitro and in vivo. *Cancer Res.*, **64**, 4875–4886.
33. Wang, L. and Duncan, G. (2006) Silencing of sigma-1 receptor induces cell death in human lens cells. *Exp. Cell. Res.*, **312**, 1439–1446.
34. Hayashi, T., Maurice, T. and Su, T.P. (2000) Ca(2+) signaling via sigma(1)-receptors: novel regulatory mechanism affecting intracellular Ca(2+) concentration. *J. Pharmacol. Exp. Ther*, **293**, 788–798.
35. Schrock, J.M., Spino, C.M., Longen, C.G., Stabler, S.M., Marino, J.C., Pasternak, G.W. and Kim, F.J. (2013) Sequential cytoprotective responses to Sigma1 ligand-induced endoplasmic reticulum stress. *Mol. Pharmacol.*, **84**, 751–762.
36. MacVicar, T.D., Mannack, L.V., Lees, R.M. and Lane, J.D. (2015) Targeted siRNA Screens Identify ER-to-Mitochondrial Calcium Exchange in Autophagy and Mitophagy Responses in RPE1 Cells. *Int. J. Mol. Sci.*, **16**, 13356–13380.
37. Kwok, A.S., Phadwal, K., Turner, B.J., Oliver, P.L., Raw, A., Simon, A.K., Talbot, K. and Agashe, V.R. (2011) HspB8 mutation causing hereditary distal motor neuropathy impairs lysosomal delivery of autophagosomes. *J. Neurochem.*, **119**, 1155–1161.
38. Nixon, R.A. (2013) The role of autophagy in neurodegenerative disease. *Nat. Med.*, **19**, 983–997.
39. Maurice, T. and Su, T.P. (2009) The pharmacology of sigma-1 receptors. *Pharmacol. Ther.*, **124**, 195–206.
40. Seelow, D., Schuelke, M., Hildebrandt, F. and Nurnberg, P. (2009) HomozygosityMapper–an interactive approach to homozygosity mapping. *Nucleic Acids Res.*, **37**, W593–W599.
41. Albrechtsen, A., Sand Korneliussen, T., Moltke, I., van Overseem Hansen, T., Nielsen, F.C. and Nielsen, R. (2009) Relatedness mapping and tracts of relatedness for genome-

wide data in the presence of linkage disequilibrium. *Genet. Epidemiol.*, **33**, 266–274.
42. Krumm, N., Sudmant, P.H., Ko, A., O'Roak, B.J., Malig, M., Coe, B.P., Quinlan, A.R., Nickerson, D.A. and Eichler, E.E. (2012) Copy number variation detection and genotyping from exome sequence data. *Genome Res.*, **22**, 1525–1532.
43. McKenna, A., Hanna, M., Banks, E., Sivachenko, A., Cibulskis, K., Kernytsky, A., Garimella, K., Altshuler, D., Gabriel, S., Daly, M., *et al.* (2010) The Genome Analysis Toolkit: a MapReduce framework for analyzing next-generation DNA sequencing data. *Genome Res.*, **20**, 1297–1303.
44. Schwarz, J.M., Cooper, D.N., Schuelke, M. and Seelow, D. (2014) MutationTaster2: mutation prediction for the deep-sequencing age. *Nat. Methods*, **11**, 361–362.
45. Gonzalez-Perez, A. and Lopez-Bigas, N. (2011) Improving the assessment of the outcome of nonsynonymous SNVs with a consensus deleteriousness score, Condel. *Am. J. Hum. Genet.*, **88**, 440–449.
46. Chun, S. and Fay, J.C. (2009) Identification of deleterious mutations within three human genomes. *Genome Res.*, **19**, 1553–1561.
47. Gao, X.F., Yao, J.J., He, Y.L., Hu, C. and Mei, Y.A. (2012) Sigma-1 receptor agonists directly inhibit Nav1.2/1.4 channels. *PLoS One*, **7**, e49384.
48. Granatiero, V., Giorgio, V., Cali, T., Patron, M., Brini, M., Bernardi, P., Tiranti, V., Zeviani, M., Pallafacchina, G., De Stefani, D., *et al.* (2016) Reduced mitochondrial Ca transients stimulate autophagy in human fibroblasts carrying the 13514A>G mutation of the ND5 subunit of NADH dehydrogenase. *Cell Death Differ.*, **23**, 231–241.
49. Onesto, E., Rusmini, P., Crippa, V., Ferri, N., Zito, A., Galbiati, M. and Poletti, A. (2011) Muscle cells and motoneurons differentially remove mutant SOD1 causing familial amyotrophic lateral sclerosis. *J. Neurochem.*, **118**, 266–280.
50. Hill, J.M.D., Stefani, D., Jones, A.W., Ruiz, A, Rizzuto, R. and Szabadkai, G., (2014) Measuring baseline Ca(2+) levels in subcellular compartments using genetically engineered fluorescent indicators. *Methods Enzymol.*, **543**, 47–72.
51. Schindelin, J., Arganda-Carreras, I., Frise, E., Kaynig, V., Longair, M., Pietzsch, T., Preibisch, S., Rueden, C., Saalfeld, S., Schmid, B., *et al.* (2012) Fiji: an open-source platform for biological-image analysis. *Nat. Methods*, **9**, 676–682.